Journal for ImmunoTherapy of Cancer

Clonal expansion of resident memory T cells in peripheral blood of patients with non-small cell lung cancer during immune checkpoint inhibitor treatment

Hyunsu Kim,[1,2] Sehhoon Park,[3] Kyoung-Yeon Han,[2] Naeun Lee ,[1] Hyemin Kim,[4] Hyun Ae Jung,[3] Jong-Mu Sun,[3] Jin Seok Ahn,[3] Myung-Ju Ahn,[3] Se-Hoon Lee,[1,3] Woong-Yang Park [1,2,5]

To cite: Kim H, Park S, Han K-Y, *et al*. Clonal expansion of resident memory T cells in peripheral blood of patients with non-small cell lung cancer during immune checkpoint inhibitor treatment. *Journal for ImmunoTherapy of Cancer* 2023;**11**:e005509. doi:10.1136/jitc-2022-005509

► Additional supplemental material is published online only. To view, please visit the journal online (http://dx.doi.org/10.1136/jitc-2022-005509).

HK and SP are joint first authors.

Accepted 06 December 2022

Check for updates

© Author(s) (or their employer(s)) 2023. Re-use permitted under CC BY-NC. No commercial re-use. See rights and permissions. Published by BMJ.

For numbered affiliations see end of article.

Correspondence to
Dr Woong-Yang Park; woongyang@gmail.com

Dr Se-Hoon Lee; sehoon.lee119@gmail.com

ABSTRACT

Background Immune checkpoint inhibitors (ICIs) are an essential treatment for non-small cell lung cancer (NSCLC). Currently, the tumor-related intrinsic factors in response to ICIs have mostly been elucidated in tissue samples. However, tissue immune status and changes in the immune microenvironment can also be reflected and monitored through peripheral blood.

Methods Single-cell RNA and T cell receptor (scTCR) sequencing were conducted using peripheral blood mononuclear cells (PBMCs) from 60 patients with stage IV NSCLC. Those samples were prospectively acquired from patients treated with anti-PD(L)-1 therapy for advanced lung cancer. Based on the clinical outcomes, samples were classified as durable clinical benefit (DCB) and non-durable clinical benefit (NCB). The samples constituted paired longitudinal samples, consisting of pre-treatment and on-treatment. Additionally, PBMC samples from 60 healthy donors from the Asian Immune Diversity Atlas project were used as a control.

Results The dynamic changes in major cell types between pre-treatment and on-treatment PBMCs were associated with an increase in proliferating T cells and NK cells in both DCB and NCB groups. Among T cell subtypes, effector memory $CD8^+$ T cells ($CD8^+$ T_{EM}_GZMK_PDCD1) were increased after ICI treatment in both DCB and NCB. From the lineage trajectory analysis, effector memory $CD8^+$ T cells resided at the bifurcation point, which has the potential to differentiate into lineages with precursor exhausted $CD8^+$ T cells ($CD8^+$ T_{CM} cells) assumed to be related to the ICI response. From the scTCR-seq, effector memory $CD8^+$ T cells along with T cells recognizing unknown antigen expanded and composed of novel clones skewed toward dysfunctional status, especially in on-treatment samples of the DCB group. The extent of immunophenotype conversion capabilities of the TCR with effector memory $CD8^+$ T cells showed remarkable variation in the on-treatment sample in the DCB group.

Conclusion A transitioning T cell subtype identified in PBMCs might be related to the prolonged ICI response. From our study, expansion of effector memory $CD8^+$ T cells with novel TCRs in PBMCs after ICI treatment could contribute to a better clinical outcome in patients with NSCLC. This proof-of-concept research strengthens the use of non-invasive PBMCs in studying systemic changes of immune reactions related to the ICI treatment.

WHAT IS ALREADY KNOWN ON THIS TOPIC

⇒ Resident memory T cells or tumor-infiltrating lymphocytes has been investigated as biomarkers related to the immune checkpoint inhibitor (ICI) response in tissue samples from various cancer types. However, limited data available using single-cell RNA sequencing and single-cell T cell receptor sequencing (scTCR-seq) using peripheral blood mononuclear cells (PBMC).

WHAT THIS STUDY ADDS

⇒ Novel TCR clones of $CD8^+$ T_{EM}_GZMK_PDCD1 cells and proliferating T cells were expanded on ICI treatment, which was associated with the prolonged ICI response. The clonotypes of both cell types, with large clonal size, became more dysfunctional after ICI treatment, which also shares TCRs after ICI treatment.

HOW THIS STUDY MIGHT AFFECT RESEARCH, PRACTICE OR POLICY

⇒ Expansion of $CD8^+$ T_{EM}_GZMK_PDCD1 cells evaluated from PBMC after ICI treatment could contribute to a better clinical outcome in patients with non-small cell lung cancer. In addition, our approach supports the utility of non-invasive PBMC as a potential biomarker of ICI treatment.

BACKGROUND

Immune checkpoint inhibitors (ICIs) have rapidly been changing the therapeutic landscapes for locally advanced or metastatic non-small cell lung cancer (NSCLC). ICI-based treatments are incorporated in response to the expression of programmed death-ligand 1 (PD-L1) in tumor cells and can be administered as either monotherapy or combined with conventional cytotoxic chemotherapies.[1–3]

Overall response rates and duration of ICI vary based on the PD-L1 expression.[4] However, due to the limited predictive power of PD-L1, extensive effort has been made to elucidate additional predictive biomarkers for ICIs by incorporating tissue-based genomic outcomes, including somatic alteration and transcriptomic analysis.[5] Among the biomarkers, tumor mutation burden and microsatellite instability showed clinical benefit regardless of tumor types by initiating the first step of the cancer-immunity cycle with a high possibility of presenting cancer-specific antigen.[6–8] In addition, the gene expression profile (GEP), indicative of such functions as T cell infiltration or chemotaxis, and analyzed from transcriptomic results of tumor tissues, can also partially differentiate ICI responders from non-responders.[7 9 10] Furthermore, advanced GEP analysis from bulk sequencing data, changes in systemic immune reaction after ICI treatment, and their correlation to clinical outcomes has been conducted using single-cell expression analysis from both tissue and blood.[11–14] From single-cell analysis, clonally expanded cells have been identified from peripheral blood after ICI treatment likely to derive from tumor-infiltrating lymphocytes (TILs), which reflect the immune status of the tumor microenvironment (TME). In addition, these expanded cells were mostly novel clones rather than pre-existing clones.[11–14] Despite the benefit of non-invasive acquisition of peripheral blood mononuclear cells (PBMCs) over multiple time points, these markers have been limited by insufficient data showing a positive correlation between the expanded T cell clones and the clinical outcome.

This study is designed to investigate the changes in immune systems after ICI treatment by monitoring the immune cell type proportions observed from PBMC, and by GEP analysis before and during ICI treatment. We tested our hypothesis using prospectively collected pre-treatment and on-treatment blood samples between 1 and 3 weeks after ICI treatment from patients with advanced NSCLC treated with PD-(L)1 inhibitors. Using samples collected in a paired manner, single-cell RNA-sequencing (scRNA-seq) and single-cell T cell receptor-sequencing (scTCR-seq) were performed to evaluate the changes in the proportion of immune cells and characteristics before and during the ICI treatment. Outcomes were also matched to ICI response to evaluate the predictive.

MATERIALS AND METHODS

Sample collection and clinical study

This study was conducted using PBMCs from 60 patients with stage IV NSCLC. PBMC samples from healthy donors from the Asian Immune Diversity Atlas project were used as a control. Samples were prospectively acquired from patients treated with anti-PD(L)-1 therapy (pembrolizumab, nivolumab, atezolizumab) for advanced lung cancer. The samples consisted of 26 patients with progressive disease, 22 with partial response, and 12 with stable disease defined by the response evaluation criteria in solid tumors criteria. Based on the clinical outcomes, samples with either partial response or stable disease lasting more than 6 months were classified as durable clinical benefit (DCB), while progressive or stable disease lasting less than 6 months as non-durable clinical benefit (NCB). The samples constituted paired longitudinal samples, consisting of pre-treatment (0–7 days before the PD-(L)1 therapy) and on-treatment (1–3 weeks since the start of PD-(L)1 therapy). The detailed methods for the sample preparation, procedure of scRNA-seq and scTCR-seq, and data analysis method is described in online supplemental material 1.

Definition of signature gene score

We calculated naiveness, cytotoxicity, and dysfunction score using UCell V.1.1.0[15] for the following genes commonly reported in studies[16] related to each state: six naïve markers (*TCF7*, *CCR7*, *SELL*, *LEF1*, *IL7R*, *LTB*), 6 dysfunction associated genes (*PDCD1*, *CTLA4*, *TIGIT*, *HAVCR2*, *LAG3*, *LAYN*), and eight cytotoxic markers (*CX3CR1*, *PRF1*, *GZMA*, *GZMB*, *GZMH*, *GNLY*, *KLRG1*, *NKG7*). To estimate the relationship between these scores with Slingshot lineages, we performed locally weighted scatterplot smoothing regression and calculated the Pearson correlation.

Trajectory analysis

The Slingshot[17] (V.1.8.0) package in R was used to confirm the annotation of clusters based on the differentiation process for $CD4^+$ or $CD8^+$ T cells. Also, branching lineages in those cell types were inferred separately, considering naive T cells as a state of root when calculating the pseudo-time and the trajectories.

Classification of T cells recognizing unknown antigen and virus-specific T cells

We matched CDR3 sequences of TCRs from our samples to 70,497 CDR3 sequences of that known to recognize viruses in a database called VDJdb.[18] The matched TCRs were defined as 'virus-specific T cells' and the mismatched TCRs were defined as 'T cells recognizing unknown antigen (TRUA)'.

Definition of expanded, large, contracted, other, and novel clonotypes

Using paired samples acquired from pre-treatment and on-treatment, we used practical definitions of clones, 'expanded', 'large', 'contracted', 'other', 'novel', based on the cell count using absolute value due to the reason that some clones do not show in the pre-treatment sample. We defined an 'Expanded' clone as follows: (1) an increase in the number of cells with a distinct clonotype on-treatment rather than pre-treatment and (2) the number of cells with a certain clonotype>1 on treatment. 'Large' clonotypes were defined as clonotypes with 10 or more cells identified in pre-treatment and on-treatment. 'Contracted' clonotypes were defined as clonotypes with >1 cells in pre-treatment, but with only one cell identified in the on-treatment sample—meaning that it was clonal in pre-treatment only. 'Other' clonotypes refer to clonotypes that do not meet the four predefined conditions,

Kim H, *et al*. *J Immunother Cancer* 2023;**11**:e005509. doi:10.1136/jitc-2022-005509

which included non-clonal T cells both pre-treatment and on-treatment, and clonal T cells with a higher number of cells with a specific clonotype in pre-treatment than on-treatment. Clonotypes that were not found before treatment but present in more than one cell on-treatment were called 'novel' clonotypes. Novel clonotypes were contained to a subgroup of 'expanded' clonotypes.

RESULTS

Characteristics of study population and PBMCs

PBMCs in patients with advanced NSCLC treated with ICI as monotherapy were prospectively collected. Among the patients available for the multiplex scRNA-seq, 30 patients with DCB and 30 patients with NCB were selected for the analysis (figure 1A). Among the patients, 55 patients (91.7%) were either current or formal smokers and 5 patients (8.3%) were never-smokers. The majority of patients were diagnosed with adenocarcinoma (n=29, 48%), followed by squamous cell carcinoma (n=25, 41%), and other histology (n=6, 10%). Patients received either pembrolizumab (n=33, 55%), nivolumab (n=5, 8.3%), or atezolizumab (n=22, 36.7%) as either the first line (n=14, 23.3%), second line (n=30, 50.0%), or third line and later treatments (n=16, 26.7%) (online supplemental tables 1–3). After excluding the intersample and intrasample doublet,[19] a total of 405,303 cells (mean 3,337 (range 208–6,575) cells per sample) passed the quality control process and were subsequently used for the final analysis (online supplemental figure 1A). The major cell types were broadly annotated into 17 subtypes based on their expression of canonical gene markers (figure 1B, online supplemental figure 1B).

The proportion of representative cell types on ICI treatment

The proportion of major cell types was compared according to clinical outcome and sampling time to evaluate the difference in proportion among cell types (figure 1C, online supplemental figure 1C). The analysis conducted based on clinical response (NCB vs DCB) showed no differences in the proportion of representative cell types. To evaluate the dynamic changes after the ICI treatment in both NCB and DCB samples, we analyzed the paired samples using pre-treatment and on-treatment samples. In the NCB samples, but not in the DCB samples, a decrease was observed in plasmablasts (p=0.015), B cells (p=0.031), and $CD14^+$ platelets (p=0.022) after the ICI treatment. Furthermore, the proportions of cDC2 and $CD4^+$ T cells were decreased in both the NCB and DCB samples after the ICI treatment. On the contrary, the proportion of proliferating T and NK cells was increased after ICI treatment in both the NCB and DCB samples (figure 1C,D).

The states of T cell subtypes potentially reinvigorated on ICI treatment

As a follow-up analysis, we focused on the proliferating T and NK cells, which were increased after ICI treatment in both NCB and DCB samples. We reclustered 217,629 T and NK cells and defined 19 distinct T and NK cell subtypes based on canonical and differentiation-related gene markers (figure 2A, online supplemental figure 2A).[10 20–22] We excluded 3 of 19 clusters categorized as either stress-related (C17), doublets (C18), or a mitochondria (MT)-enriched cluster (C19) for the downstream analysis due to low cellular quality. The remained 13 T cell subtype clusters and 3 NK cell subtype clusters were analyzed.

The composition of the 13 T cell clusters was compared based on their clinical outcome and time point of sample collection (figure 2B, online supplemental figure 2B). Of the T cell subtypes, five subtypes showed significant changes in proportion between ICI pre-treatment and on-treatment samples, namely proliferating T (C6), $CD8^+$ T_{CM} (C9), $CD8^+$ T_{EM}_GZMK_PDCD1 (C11), $CD4^+$ T_N (C13), and $CD4^+$ T_{CM} (C14) cells. Looking into changes based on the clinical outcomes, C13 and C14 were decreased after ICI treatments in both the DCB and NCB groups (figure 2B). The proportion of C9, characterized by expression of *TCF7* and inhibitory molecules other than *PDCD1* and *LAG3*, increased only in the DCB samples. C6 in DCB and C11 in both the NCB and DCB groups, characterized by significant upregulation of major histocompatibility complex (MHC) class II genes, increased after ICI treatment, whereas *PDCD1* and *LAG3* were highly upregulated in the on-treatment samples compared with pre-treatment samples (figure 2B,C, online supplemental figure 2A).

To elucidate the characteristics of the cell types, we categorized the aforementioned 13 T cell subtypes into 5 groups based on their expression of gene sets representing the immunophenotypes of naïve-like, cytotoxic, transitional, dysfunctional,[16] and tissue-resident memory T (T_{RM}) cells[22] through hierarchical clustering (figure 2C). Gene markers of the naïve-like state group, represented by *TCF7, CCR7*, and *SELL* expression, were abundant in $CD8^+$ T_N cells (C8), C9, and three $CD4^+$ T cell clusters (C13, C14, C16). Among the naïve-like state group, C9 also had upregulated *GZMK*, *TIGIT*, *HAVCR2*, and *CTLA4* genes which were corresponded to the gene sets for transitional and dysfunctional state groups.[16] C6 and C11 were enriched with cytotoxic-related genes, *GZMH, CX3CR1, PRF1*, and *GZMB*. Simultaneously, both clusters had high expression of immune checkpoint molecules (*PDCD1* and *LAG3*), *ENTPD1, ZNF683,* and *ITGAE* genes which were previously reported to be upregulated in T_{RM}.[10 20–23] In addition, both clusters were downregulated in tumor necrosis factor (*TNF*) and *IL2RA*, which was also concordant with previous findings observed in tumor-specific $CD8^+$ TILs from lung cancer and melanoma.[21–23] Interestingly, the dysfunction score was increased in the C11 in the on-treatment samples, while the cytotoxic score remained high in both ICI pre-treatment and on-treatment samples (online supplemental figure 2C,D). Based on this pattern, we categorized both C6 and C11 as 'T cells in transition'—an intermediate stage of dysfunctional states.

Three NK cell clusters were composed of $CD56^{high}$ NK cells (C1), $CD56^{low}$ NK cells (C2), and $CD56^{low}$ NK_IFNG

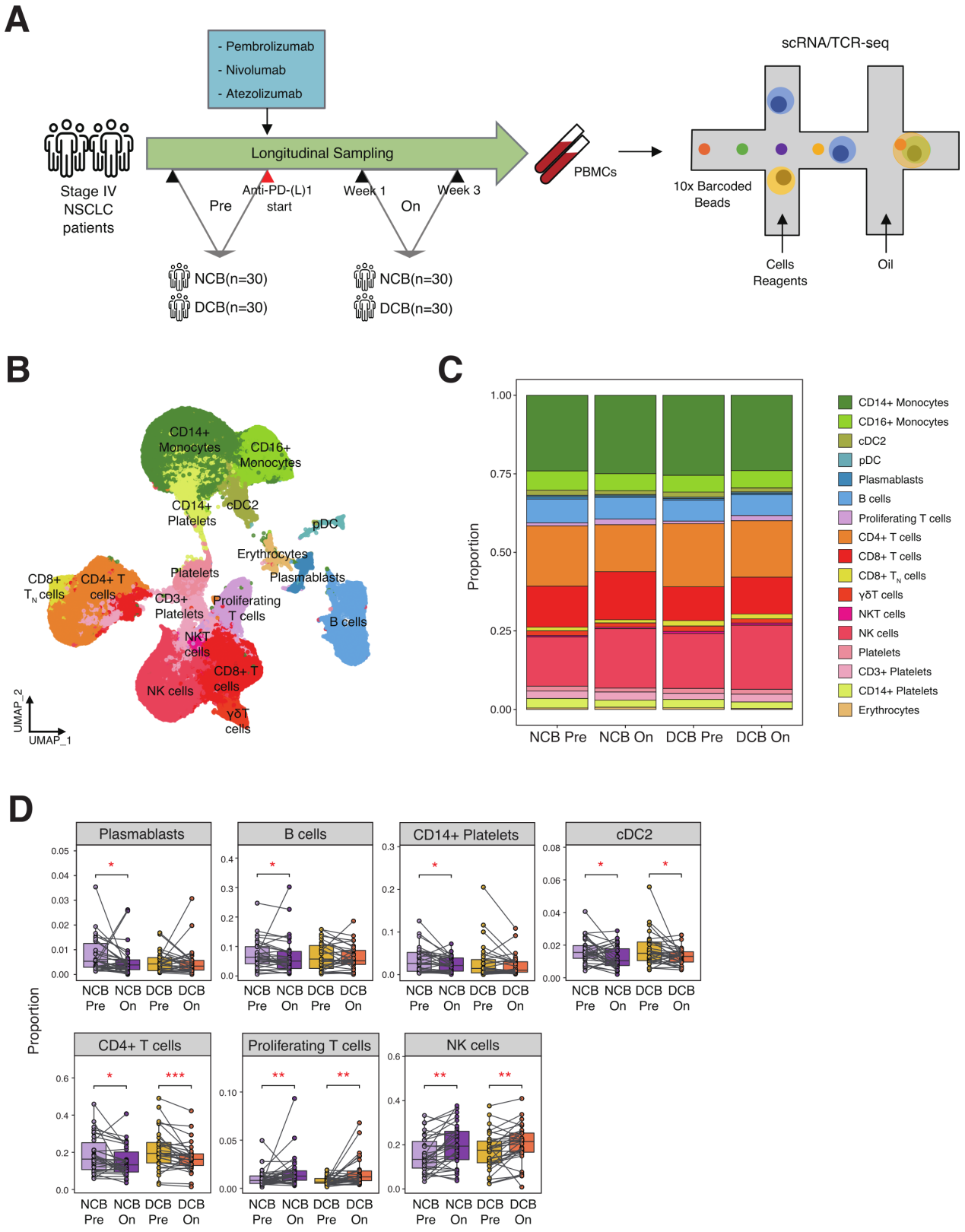

Figure 1 Overview of study and analysis of representative cell types on immune checkpoint inhibitor (ICI) treatment. (A) Scheme of the overall study design. Peripheral blood mononuclear cells from stage IV non-small cell lung cancer patients (n=60) before and after ICIs were sequenced by 5' scRNA and scTCR sequencing. (B) UMAP indicating cell types of 405,303 analyzed cells pre-treatment and on-treatment. (C) Bar plot showing distribution of subclusters from global cell types based on the clinical response (NCB and DCB) and the sampling time point (pre-treatment and on-treatment). (D) Box plot indicating proportion of cell types based on response (NCB=30, DCB=30) and sampling time point (pre-treatment=30, on-treatment=30). *p<0.05; **p<0.01; ***p<0.001; using Wilcoxon rank sum and signed-rank tests. DCB, durable clinical benefit; NCB, non-durable clinical benefit; NSCLC, non-small cell lung cancer; scTCR, single-cell T cell receptor.

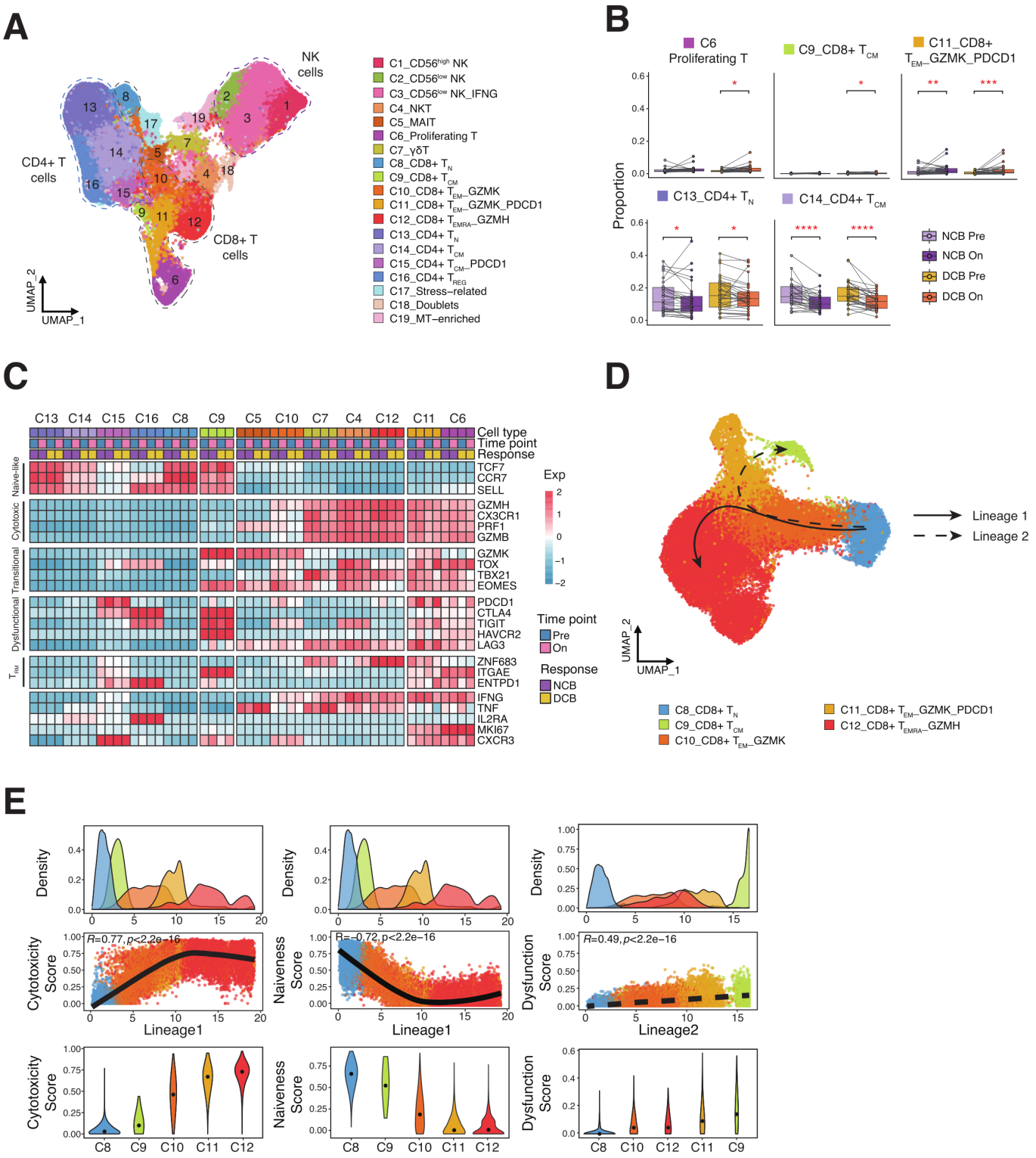

Figure 2 State of T and NK cell subtypes and lineage analysis of CD8+ T cells. (A) UMAP visualization of 217 629 T cells and NK cells based on gene expression profile. The color legend applies to B–E. T_N, naive T; T_{CM}, central memory T; T_{EM}, effector memory T; T_{EMRA}, terminally differentiated effector memory T; T_{REG} regulatory T cells. (B) Box plot showing the proportion of T cell subtypes based on clinical response and the sampling time point. *p<0.05; **p<0.01; ***p<0.001; ****p<0.0001; using Wilcoxon rank sum and signed-rank tests. (C) Heatmap indicates differential expression of selected genes by cell type. Z-score with range –2 to 2 from blue to red. Selected genes are grouped as naive-like, cytotoxic, transitional, dysfunctional, and TRM-associated. (D) Pseudo-time trajectories of CD8+ T cells. Two different trajectories were composed with different CD8+ T cell phenotypes from C8 to C12. (E) Density and correlation of pseudotime with cytotoxicity, naiveness, and dysfunction scores. Density plot displays density of CD8+ T cell subtypes at each lineage point. Solid black line and the top-left text (R) denote LOESS fit and Pearson's correlation, respectively. Distribution of functional scores for each cluster was plotted on a violin plot. DCB, durable clinical benefit; NCB, non-durable clinical benefit.

cells (C3) (figure 2A). There were no differences in the proportion of clusters between the NCB and DCB samples. However, the proportion of C1 was increased after ICI treatment regardless of clinical response, and that of C3 was increased after ICI treatment only in the DCB group (online supplemental figure 2A,E).

Define CD8$^+$ T_{EM}_GZMK_PDCD1 cells (C11) as 'T cells in transition' through lineage trajectory analysis

To characterize the cytotoxic T cells expressing gene sets of the 'transition' and 'dysfunction' status groups, we computationally inferred differentiation lineages of T cells using Slingshot.[17] The pseudotime analysis conducted using CD8$^+$ T cell clusters showed a clear separation between cytotoxic and dysfunctional status T cells. CD8$^+$ T_N cells (C8) were connected to CD8$^+$ T_{EM}_GZMK cells (C10) and then to CD8$^+$ T_{EM}_GZMK_PDCD1 cells (C11). After that, C11 branched into two different trajectories forming terminally differentiated CD8$^+$ T_{EMRA}_GZMH cells (C12) and CD8$^+$ T_{CM} cells (C9), named lineage 1 and 2, respectively (figure 2D). Lineage 1 showed a strong positive correlation with the cytotoxicity score and a negative correlation with the naiveness score. Lineage 2 showed a moderate association with the dysfunction score (figure 2E). C11 resided midway in the trajectories maintaining both cytotoxic and dysfunctional characteristics as 'T cells in transition' (figure 2D).

In analyzing CD4$^+$ T cells clusters, we observed a single trajectory beginning in CD4$^+$ T_N cells (C13), progressing toward CD4$^+$ T_{CM} cells (C14) and CD4$^+$ T_{CM}_PDCD1 cells (C15), before ending in CD4$^+$ T_{REG} cells (C16) (online supplemental figure 2F). The lineage indicated moderately negative correlations with the naiveness score toward C16, but weak correlations with the cytotoxicity and dysfunction scores (online supplemental figure 2G).

Features of expanded clonotypes in lung cancer population vs. healthy population

Using scTCR-seq, we investigated the expansion of T cell clonotypes based on the functional states of cell types. We analyzed TCRs with either alpha or beta chains from 127,843 cells matched with scRNA-seq data in PBMCs (figure 3A, online supplemental figure 3A). A TCR was classified as a clonal TCR if the same clonotype was observed in more than 1 cell (n=35,330), of which up to 7% of clonotypes were categorized as clonal TCRs which were mostly enriched in the CD8$^+$ T cells (figure 3B,C). Other cells with no clonal TCRs were dominated by the cell types with naïve-like state immunophenotypes.

To understand the dimension of T cell heterogeneity in normal samples without lung cancer, we analyzed 104,111 T and NK cells from the PBMCs of 60 healthy donors. Overall cell types in healthy donors showed a higher proportion of naïve-like state cell types, such as CD8$^+$ T_N, CD4$^+$ T_N, and CD4$^+$ T_{CM}, compared with the cell types of our study population (online supplemental figure 3B). On the contrary, more cell types with dysfunctional and cytotoxic characteristics such as CD56^{low} NK and CD8$^+$ T_{EM}_GZMH were observed in our study population. Although the CD8$^+$ T cell clusters similarly accounted for a greater proportion of clonal TCRs rather than CD4$^+$ T cell clusters in healthy individuals, the proportion of overall clonal TCRs were lower in the healthy individuals, showing less than 4% enrichment (figure 3B,C, online supplemental figure 3C).

Features of clonotype in TRUA versus virus-specific T cells

To evaluate whether the subpopulation of T cells which recognize tumor-associated antigen was likely to expand after the ICI treatment, we defined clonotypes into four classes (expanded, contracted, large, and others) (online supplemental figure 3D). In particular, we distinguished T cells into two groups: TRUA and virus-specific T cells. TRUA accounted for ~89.7% of total T cells (online supplemental figure 3E). Expanded clonotypes in TRUA were slightly enriched in the NCB group compared with the DCB group (2.7% vs 2.2%) (figure 3D). The distribution of T cell subclusters in TRUA and virus-specific T cells was calculated (online supplemental figure 3F). The expansion of TRUA clones after ICI treatment was more abundant in the cell types CD4$^+$ T cells (C13–C16), CD8$^+$ T_{EM}_GZMK_PDCD1 (C11), and proliferating T cells (C6) in the DCB group, although a similar trend was observed in the NCB group. In virus-specific T cell clones, these cell types were expanded after ICI treatment prominently in the NCB group (figure 3E).

Gini index[24] and TCR richness[25] were calculated by T cell subclusters to quantify the abundance of clonotypes or diversity in each sample. The Gini index, or clonality, was higher in the majority of CD8$^+$ T cell clusters (online supplemental figure 3G). Although the Gini index tended to increase in both the NCB and DCB groups after the ICI treatment, there was no significant difference in the Gini index based on the treatment response (online supplemental figure 3H). For further analysis, we designated the 'novel' clonotype as a clonotype not detected in pretreatment samples but newly identified in the on-treatment samples. In virus-specific T cells, novel clonotypes were more frequent in the NCB group (61.6%) compared with the DCB group (55.0%). On the contrary, novel clonotypes were similar in the TRUA clones in both the NCB and DCB group (56.2% vs 56.1%) (online supplemental figure 3I). However, a detailed analysis of cellular subtypes showed novel clonotypes from the TRUA clones in C6 and C11 were higher in the DCB group (69.7% and 57.6%, respectively) compared with the NCB group (50.0% and 40.1%, respectively) (online supplemental figure 3J).

Changes in clonal size of novel T cells and correlation to ICI treatment response

To delineate the relationship between the characteristics of antitumor CD8$^+$ T cells and the response to ICI treatment, we investigated the changes of the clonality by comparing the size of clones (figure 4A). We identified a significant expansion of TRUA clones after ICI

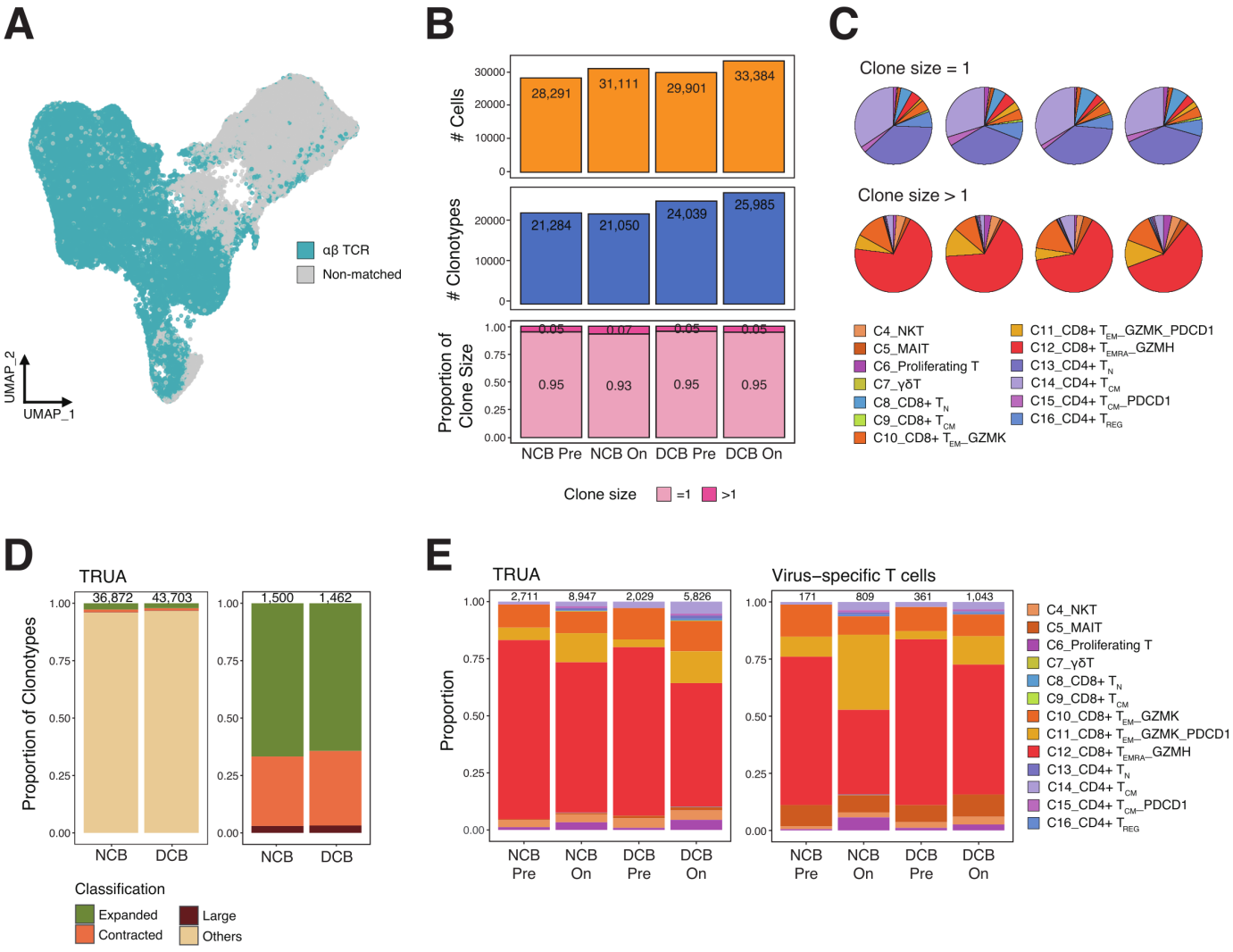

Figure 3 States of expanded clones in TRUA and virus-specific T cells. (A) T and NK cells (127 843 total) were matched based on TCRs alpha or beta chain. (B) Clonal composition of T cells indicating the number of T cells obtained from TCR, the number of unique clonotypes, and the distribution of clonotypes along clonal sizes. (C) Pie charts indicating the cell type composition based on clinical response and sampling time point. (D) TRUA clonotypes classified four groups (expanded, contracted, large, and others). Proportion of these TRUA clonotypes was calculated based on clinical outcome. The right bar graph reflects the proportion of TRUA clonotypes excluding the 'others' group. The number at the top of the bar plot indicates total TRUA clonotypes. (E) The proportion of cell types constituting expanded TRUA and virus-specific T cell clones. DCB, durable clinical benefit; NCB, non-durable clinical benefit; TCR, T cell receptor; TURA, T cells recognizing unknown antigen.

treatment, many of which were occupied by proliferating T cells (C6) and CD8$^+$ T_{EM}_GZMK_PDCD1 cells (C11) with higher cytotoxicity score than the dysfunction score. Moreover, expanded C6 and C11 after ICI treatment were mostly derived from novel clonotypes. Comparing the size of novel clones expanded after ICI treatment based on the clinical response, expansion was more prominent in the DCB group compared with the NCB group (figure 4A). Given the relationship between the dysfunction score and size of TRUA clones, we hypothesized that TRUA clones in a transitional state, such as C6 and C11 of pre-treatment samples may increase in clonal size and dysfunction score after ICI treatment—especially in the DCB group. We investigated the difference in all cell types based on a cut-off (0.171) of the dysfunction score in TRUA clones and categorically classified them into 'predysfunction' (≤0.171) and 'dysfunction' (>0.171) (figure 4B, online supplemental figure 4A). In the on-treatment samples of the DCB group, there was a statistically significant increase in clonal size of C6 and C11 toward the 'dysfunction' state after ICI treatment, many of which derived from novel clonotypes (figure 4C). On the contrary, other T cell subpopulations in TRUA showed decreased or insignificant changes (online supplemental figure 4B). This finding indicated difference in the pattern of clonal expansion between NCB and DCB after ICI treatment. A similar pattern was observed in C6 and C11 in virus-specific T cell clones showing no statistical difference in clonal size (figure 4A, online supplemental figure 4C,D). However, among the virus-specific T cell clones, the T cell clonotypes with large clonal sizes in the on-treatment samples from both NCB and DCB groups

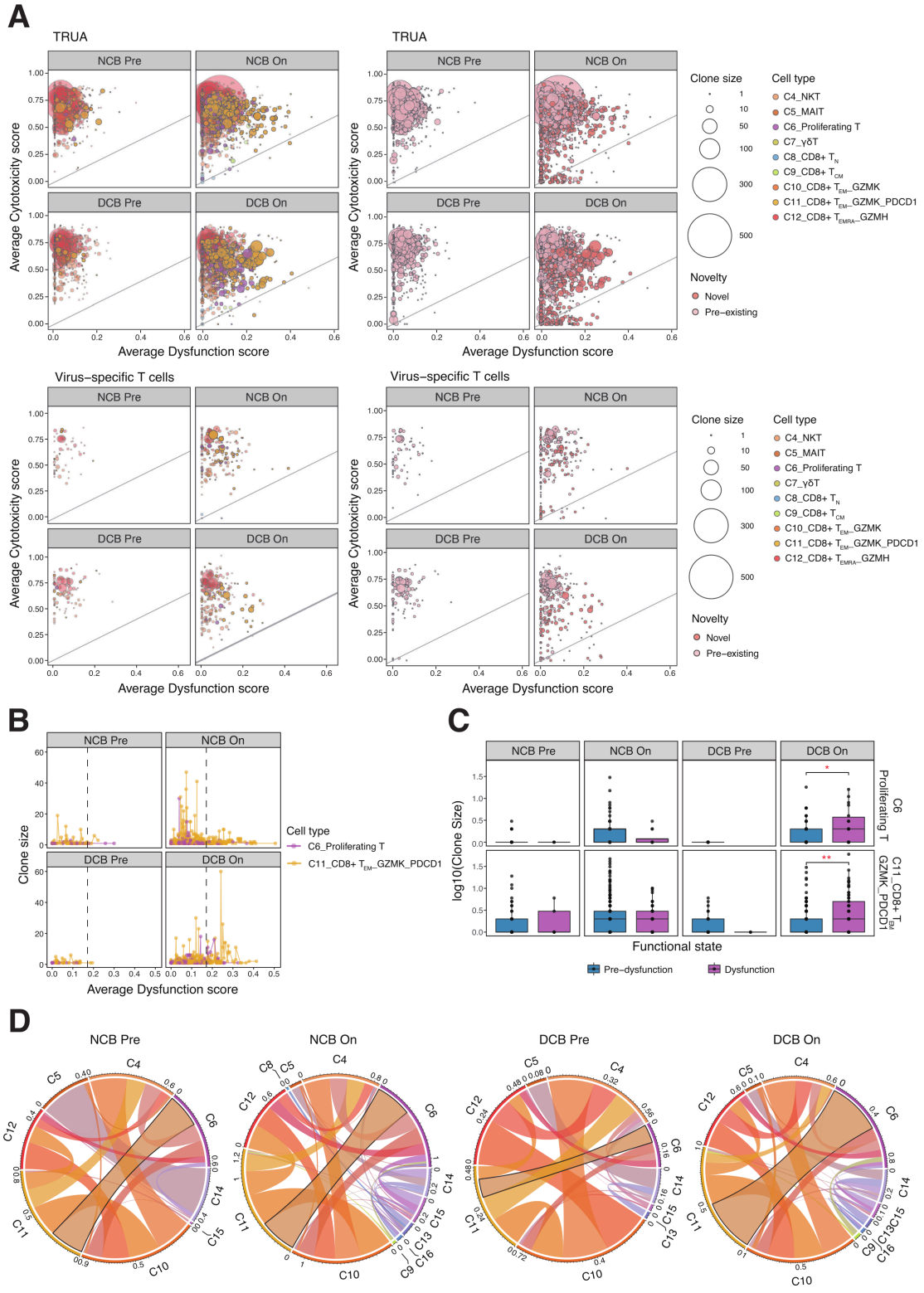

Figure 4 Dysfunction score and clone size of T cells in transitional state in response to ICI. (A) Bubble plots indicating size of clones and the characteristics of cell types. Changes in cytotoxic and dysfunction score based on the cell types (top, left) and novelty (top, right) in TRUA. Similarly, cell types (bottom, left) and novelty (bottom, right) in virus-specific T cells. (B) Size distribution of TCR clones with proliferating T cells and $CD8^+$ T_{EM}_GZMK_PDCD1 based on the average value of dysfunction score. Line color shows subtypes of T cells. Each dot represents a single clone by sample. (C) Clone size were compared based on functional states (predysfunction, dysfunction) using dysfunction score cut-off 0.171. *p<0.05; **p<0.01; using Wilcoxon rank sum tests. (D) The extent of sharing TCRs between T cell subtypes. Sectors of circos plot indicate immunophenotypes of the shared TCR. Links represent the interaction between T cell subtypes. The width of links is the degree of transition calculated by STARTRAC. DCB, durable clinical benefit; ICI, immune checkpoint inhibitor; NCB, non-durable clinical benefit; TCR, T cell receptor; TRUA, T cells recognizing unknown antigen.

were significantly enriched in CD8$^+$ T_{EMRA}_GZMH cells (C12) which were derived from pre-existing clonotypes (figure 4A). The majority of clones in the CD4$^+$ T cells were derived from novel clones after ICI treatment in both TRUA and virus-specific T cells (online supplemental figures 3J,4E). The association between immunophenotypes was determined to assess the interaction between T cell clonotypes based on clinical outcome. In C6 and C11, the extent of the immunophenotype conversion capabilities of TCRs showed remarkable variation in the on-treatment samples in the DCB group compared with the NCB group (figure 4D). Looking into the number of clones sharing TCRs in C6 and C11, the number was higher in the NCB group compared with the DCB group. Similarly, clones sharing TCRs were more enriched in the on-treatment samples compared with the pre-treatment samples (online supplemental figure 4F). Furthermore, C6 that share TCRs with CD8$^+$ T_{EM}_GZMK_PDCD1 cells (C11) were subclustered. Clones with CD8$^+$ T_{EM}_GZMK_PDCD1 cells in subclusters of C6 (ProSC) were more shared in the on-treatment samples in the DCB group (online supplemental figure 4G, online supplemental figure 5A-C).

DISCUSSION

In this study, we analyzed the relevance of T cell clones in response to ICI treatment using prospectively collected PBMCs samples from patients with NSCLC who received either PD-1 or PD-L1 inhibitors. In addition, the changes in the immune system after ICI treatment were analyzed at single-cell resolution. Through a stepwise approach, we observed that the proportion of certain cell types in PBMCs changed after ICI treatment. Especially, cell types at the forefront of the immune system such as CD4$^+$ T cells, myeloid cells, and B cell-family clusters showed a decrease in their proportion after ICI treatment while the proportion of proliferating T and NK cells with upregulated cytotoxic genes increased (figure 1D). Furthermore, when the T and NK cells were reclustered into subgroups, it revealed an increase in CD8$^+$ T cells clusters (C6, C9, C11) and NK cells clusters (C1, C3) after ICI treatment (figure 2B, online supplemental figure 2E).

Among the subclusters of CD8$^+$ T cells, we focused on proliferating T cells (C6) and CD8$^+$ T_{EM}_GZMK_PDCD1 cells (C11). These cells were characterized by an increase in dysfunctional score represented by increased ICIs expression, such as *PDCD1*, *TIGIT*, *CTLA4*, and *LAG3* (online supplemental figure 2A,D). Simultaneously, these clusters showed high proliferative capacity, upregulated *MKI67*, and increased cytotoxicity scores compared with other cell types. Hence, it can be inferred that these cells are likely to be exhausted T-cells—though not terminally exhausted T-cells—which can be reinvigorated after ICI treatment.[26 27] Furthermore, it can be assumed that reinvigorated T cells might be detected in PBMCs in higher proportion after ICI treatment by promoting self-renewal and clonal expansion by unleashing the inhibitory signals derived from immune checkpoint modulation. This in turn explains the increase in the proportion of proliferating T cells (C6) and CD8$^+$ T_{EM}_GZMK_PDCD1 cells (C11) after ICI treatment observed in our study population (figure 2B).

We observed a lineage progression of CD8$^+$ T cells into two different cell types using trajectory analysis: CD8$^+$ T_{EMRA}_GZMH cells (C12) (linage 1) and CD8$^+$ T_{CM} cells (C9) (linage 2) (figure 2D). For linage 1, CD8$^+$ T_{EMRA}_GZMH cells (C12) were highly upregulated in cytotoxic genes and occupied a substantial portion of the TCR population.[14] CD8$^+$ T_{EMRA}_GZMH cells (C12) were low in gene markers related to transitional and dysfunctional states (figure 2C) and demonstrated no significant difference in cell type proportion based on clinical outcomes, although TCR clonotypes were expanded to a larger extent in NCB rather than DCB after ICI treatment. Our assumption is also supported by earlier studies that patients with high CD39$^-$ CD8$^+$ T cells, likened to CD8$^+$ T_{EMRA}_GZMH cells (C12), are unresponsive to anti-PD-1 treatment.[22 23] Therefore, CD8$^+$ T_{EMRA}_GZMH cells (C12) can be a bystander in terms of treatment response.[23] On the contrary, for linage 2, CD8$^+$ T_{CM} cells (C9) barely expressed terminally exhausted phenotypes-related genes such as *ENTPD1* (encoding CD39), *PDCD1*, and *CD69*, while expressing naïve markers such as *TCF7*, *SELL*, *CCR7* (figure 2C).[21 28 29] This resembles the gene expression pattern of precursor exhausted CD8$^+$ T (T_{PE}) cells rather than terminally exhausted T (T_{TE}) cells, thus still having the potential to reinvigorate on ICI treatment,[30] which explains the significant increase in its proportion in DCB. Previous studies have reported a high frequency of T_{PE} in tumor tissue in patients with a durable response or longer progression-free survival.[21 28–31] Hence, although CD8$^+$ T_{CM} cells (C9) accounted for only ~1% of total T cells in our dataset analyzed from PBMCs, it can be assumed that the increase of CD8$^+$ T_{CM} cells (C9) is more likely related to favorable clinical outcomes to ICIs. The CD8$^+$ T_{EM}_GZMK_PDCD1 cells (C11), which correspond to the bifurcation of the two lineages, expressed genes, such as *GZMK*, *ZNF683*, and *PDCD1*. Those genes were also expressed in clusters that suggested as 'pre-exhaustion' state and were more abundant in NSCLC tumors.[10]

To elucidate the dynamics in clonotypes we analyzed TCRs using scTCR-seq. The clonotypes which expanded in DCB after ICI treatment in TRUA were generated from novel clones. Furthermore, among these expanded clonotypes, TCR clonotypes with large clonal size and skewed toward dysfunctional status after ICI treatment were enriched in proliferating T cells (C6) and CD8$^+$ T_{EM}_GZMK_PDCD1 cells (C11) (figure 4A–C). Referring to a previous report conducted in tumor tissue that showed TCRs of clonally expanded TILs after ICI treatment were novel TCRs,[11–14] it can be hypothesized that novel clones of proliferating T cells (C6) and CD8$^+$ T_{EM}_GZMK_PDCD1 cells (C11) detected from our PBMCs were likely to the circulating immune cell-derived from expanded TILs after ICI treatment. In addition, the proliferative capacity of CD8$^+$ T_{EM}_GZMK_PDCD1 cells (C11)

that are thought to be reinvigorate through ICIs might determine the clinical outcome. Proliferating T cells (C6) and CD8$^+$ T_{EM}_GZMK_PDCD1 cells (C11) shared clones but changes in the TCR sharing pattern of both cell types were prominent in the on-treatment samples of DCB (figure 4D). These might suggest self-renewal degree of CD8$^+$ T_{EM}_GZMK_PDCD1 cells (C11) after ICI treatment can be affect the clinical outcomes.

Certain questions still need to be validated through further functional studies. The exact function of T cells in the middle of dysfunctional states, for example, CD8$^+$ T_{EM}_GZMK_PDCD1 cells (C11), remains uncertain. In addition, our analysis was only conducted using PBMC samples; thus, only limited inference can be made between TCR repertoires from the PBMCs and the TME. Lastly, our sample collection was conducted at time points between 1 and 3 weeks after ICI treatment which may be regarded as premature to fully assess the clinical outcomes. Nevertheless, our data support that CD8$^+$ T_{EM}_GZMK_PDCD1 cells (C11) identified from PBMCs resemble TILs or T_{RM}-like characteristics, which show the possibility to function as effective antitumor T cells.[21 22] Moreover, the novel clones generated after ICI treatment were enriched with CD8$^+$ T_{EM}_GZMK_PDCD1 cells (C11) which might be essential for the prolonged response of ICIs. Lastly, our findings in PBMCs support the potential utility of this approach in understanding the systemic changes in an immune reaction as well as in the TME-related clinical response of ICIs.[13] In this study, patients with never-smoker and possessing EGFR mutation are included. Due to the high rates primary resistance to ICI in theses subset, these patients might be distinct in immune profile compared with the smoker or patient without oncogene-driven mutation. However, all these patients were included after the matched target treatment, if available, and receive the ICI treatment per current standard guideline. The difference in changes of systemic immune profile before and after the ICI treatment based on mutational status and smoking need to be validate with further study. Last but not least, the antigen recognized by CD8$^+$ T_{EM}_GZMK_PDCD1 cells (C11) was not clearly defined in this study. For this reason, we used the terminology TRUA throughout the analysis. Although several tools, such as POPISK,[32] NetTCR,[33] and TCRMatch,[34] have been developed to predict the binding affinity between TCR and the corresponding epitope loaded into MHC in NSCLC patients. However, the performance of these tools is still in the development stage due to insufficient data. Therefore, the binding affinity between TCR and peptide-MHC shown in our study need to be warranted through further experimental investigations.

In conclusion, we observed the dynamic changes in systemic immune profiles using paired PBMC samples from patients who received ICI treatment. In detail, novel clones of CD8$^+$ T_{EM}_GZMK_PDCD1 cells (C11) in TRUA were expanded on ICI treatment. This event was associated with the long-term ICI response. The unique findings observed in our study, including the changes in dysfunctional status and the sharing of TCR immunophenotypes after ICI treatment should be further investigated.

Author affiliations
[1]Department of Health Sciences and Technology, SAIHST, Sungkyunkwan University, Seoul, The Republic of Korea
[2]Samsung Genome Institute, Samsung Medical Center, Seoul, The Republic of Korea
[3]Division of Hematology-Oncology, Department of Medicine, Samsung Medical Center, Sungkyunkwan University School of Medicine, Seoul, The Republic of Korea
[4]Department of Medicine, Samsung Medical Center, Sungkyunkwan University School of Medicine, Seoul, The Republic of Korea
[5]Department of Molecular Cell Biology, Sungkyunkwan University School of Medicine, Seoul, The Republic of Korea

Twitter Hyunsu Kim @Hyunsu1009

Acknowledgements We used single cell RNA sequencing data from Asian Immune Diversity Atlas (AIDA) project for healthy Korean donors. We appreciate all the members in Samsung Genome Institute for their technical and scientific discussion on this manuscript.

Contributors HK and SP interpreted the genomic and clinical data of lung cancer patients and was a major contributor of manuscript writing. K-YH, NL and HK managed patient samples for single cell analysis. HAJ, J-MS, JSA, M-JA and S-HL recruited patients for this clinical study and summarized clinical data. W-YP and S-HLacting as guarantor played a leading role of study design and manuscript. All authors approved the manuscript.

Funding This work was supported by the Bio & Medical Technology Development Program of the National Research Foundation of Korea (NRF) funded by the Korea government (MSIT) (No. 2017M3A9A7050803 to W-YP, 2020R1A2C3006535 to S-HL), the National Cancer Center Grant (NCC1911269-3 to S-HL), the Future Medicine 20*30 Project of the Samsung Medical Center (SMX1220091 to S-HL), and the Korea Health Technology R&D Project through the Korea Health Industry Development Institute (KHIDI), funded by the Ministry of Health & Welfare, Republic of Korea (grant No: HR20C0025 to S-HL).

Competing interests S-HL reports grants and personal fees from MSD, personal fees from Novartis, personal fees from AstraZeneca, personal fees from BMS, personal fees from Roche, outside the submitted work. W-YP is a founder and CEO of Geninus Inc. All remaining authors have declared no conflicts of interest.

Patient consent for publication Consent obtained directly from patient(s).

Ethics approval This study involves human participants and was approved by Samsung Medical Center Institutional Review Board (No. 2018-04-048). Participants gave informed consent to participate in the study before taking part.

Provenance and peer review Not commissioned; externally peer reviewed.

Data availability statement All data relevant to the study are included in the article or uploaded as online supplemental information.

Supplemental material This content has been supplied by the author(s). It has not been vetted by BMJ Publishing Group Limited (BMJ) and may not have been peer-reviewed. Any opinions or recommendations discussed are solely those of the author(s) and are not endorsed by BMJ. BMJ disclaims all liability and responsibility arising from any reliance placed on the content. Where the content includes any translated material, BMJ does not warrant the accuracy and reliability of the translations (including but not limited to local regulations, clinical guidelines, terminology, drug names and drug dosages), and is not responsible for any error and/or omissions arising from translation and adaptation or otherwise.

Open access This is an open access article distributed in accordance with the Creative Commons Attribution Non Commercial (CC BY-NC 4.0) license, which permits others to distribute, remix, adapt, build upon this work non-commercially, and license their derivative works on different terms, provided the original work is properly cited, appropriate credit is given, any changes made indicated, and the use is non-commercial. See http://creativecommons.org/licenses/by-nc/4.0/.

ORCID iDs
Naeun Lee http://orcid.org/0000-0002-9172-2732
Woong-Yang Park http://orcid.org/0000-0003-4234-0380

REFERENCES

1 Reck M, Rodríguez-Abreu D, Robinson AG, *et al*. Five-Year outcomes with pembrolizumab versus chemotherapy for metastatic non-small-cell lung cancer with PD-L1 tumor proportion score ≥ 50. *J Clin Oncol* 2021;39:2339–49.
2 Paz-Ares L, Ciuleanu T-E, Cobo M, *et al*. First-line nivolumab plus ipilimumab combined with two cycles of chemotherapy in patients with non-small-cell lung cancer (CheckMate 9LA): an international, randomised, open-label, phase 3 trial. *Lancet Oncol* 2021;22:198–211.
3 Hellmann MD, Paz-Ares L, Bernabe Caro R, *et al*. Nivolumab plus ipilimumab in advanced non-small-cell lung cancer. *N Engl J Med* 2019;381:2020–31.
4 Yi M, Jiao D, Xu H, *et al*. Biomarkers for predicting efficacy of PD-1/PD-L1 inhibitors. *Mol Cancer* 2018;17:129.
5 Pilard C, Ancion M, Delvenne P, *et al*. Cancer immunotherapy: it's time to better predict patients' response. *Br J Cancer* 2021;125:927–38.
6 Marabelle A, Fakih M, Lopez J, *et al*. Association of tumour mutational burden with outcomes in patients with advanced solid tumours treated with pembrolizumab: prospective biomarker analysis of the multicohort, open-label, phase 2 KEYNOTE-158 study. *Lancet Oncol* 2020;21:1353–65.
7 McKean WB, Moser JC, Rimm D, *et al*. Biomarkers in precision cancer immunotherapy: promise and challenges. *Am Soc Clin Oncol Educ Book* 2020;40:e275–91.
8 Chen DS, Mellman I. Oncology meets immunology: the cancer-immunity cycle. *Immunity* 2013;39:1–10.
9 Keenan TE, Burke KP, Van Allen EM. Genomic correlates of response to immune checkpoint blockade. *Nat Med* 2019;25:389–402.
10 Guo X, Zhang Y, Zheng L, *et al*. Global characterization of T cells in non-small-cell lung cancer by single-cell sequencing. *Nat Med* 2018;24:978–85.
11 Forde PM, Chaft JE, Smith KN, *et al*. Neoadjuvant PD-1 blockade in resectable lung cancer. *N Engl J Med* 2018;378:1976–86.
12 Yost KE, Satpathy AT, Wells DK, *et al*. Clonal replacement of tumor-specific T cells following PD-1 blockade. *Nat Med* 2019;25:1251–9.
13 Valpione S, Galvani E, Tweedy J, *et al*. Immune-awakening revealed by peripheral T cell dynamics after one cycle of immunotherapy. *Nat Cancer* 2020;1:210–21.
14 Fairfax BP, Taylor CA, Watson RA, *et al*. Peripheral CD8$^+$ T cell characteristics associated with durable responses to immune checkpoint blockade in patients with metastatic melanoma. *Nat Med* 2020;26:193–9.
15 Andreatta M, Carmona SJ. UCell: robust and scalable single-cell gene signature scoring. *Comput Struct Biotechnol J* 2021;19:3796–8.
16 van der Leun AM, Thommen DS, Schumacher TN. CD8$^+$ T cell states in human cancer: insights from single-cell analysis. *Nat Rev Cancer* 2020;20:218–32.
17 Street K, Risso D, Fletcher RB, *et al*. Slingshot: cell lineage and pseudotime inference for single-cell transcriptomics. *BMC Genomics* 2018;19:477.
18 Bagaev DV, Vroomans RMA, Samir J, *et al*. VDJdb in 2019: database extension, new analysis infrastructure and a T-cell receptor motif compendium. *Nucleic Acids Res* 2020;48:D1057–62.
19 McGinnis CS, Murrow LM, Gartner ZJ. DoubletFinder: doublet detection in single-cell RNA sequencing data using artificial nearest neighbors. *Cell Syst* 2019;8:329–37.
20 Pauken KE, Shahid O, Lagattuta KA, *et al*. Single-cell analyses identify circulating anti-tumor CD8 T cells and markers for their enrichment. *J Exp Med* 2021;218. doi:10.1084/jem.20200920. [Epub ahead of print: 05 Apr 2021].
21 Oliveira G, Stromhaug K, Klaeger S, *et al*. Phenotype, specificity and avidity of antitumour CD8$^+$ T cells in melanoma. *Nature* 2021;596:119–25.
22 Caushi JX, Zhang J, Ji Z, *et al*. Transcriptional programs of neoantigen-specific TIL in anti-PD-1-treated lung cancers. *Nature* 2021;596:126–32.
23 Simoni Y, Becht E, Fehlings M, *et al*. Bystander CD8$^+$ T cells are abundant and phenotypically distinct in human tumour infiltrates. *Nature* 2018;557:575–9.
24 Thomas PG, Handel A, Doherty PC, *et al*. Ecological analysis of antigen-specific CTL repertoires defines the relationship between naive and immune T-cell populations. *Proc Natl Acad Sci U S A* 2013;110:1839–44.
25 Zhu W, Germain C, Liu Z, *et al*. A high density of tertiary lymphoid structure B cells in lung tumors is associated with increased CD4$^+$ T cell receptor repertoire clonality. *Oncoimmunology* 2015;4:e1051922.
26 Quatrini L, Mariotti FR, Munari E, *et al*. The immune checkpoint PD-1 in natural killer cells: expression, function and targeting in tumour immunotherapy. *Cancers* 2020;12. doi:10.3390/cancers12113285. [Epub ahead of print: 06 11 2020].
27 Kim KH, Kim CG, Shin E-C. Peripheral blood immune cell-based biomarkers in anti-PD-1/PD-L1 therapy. *Immune Netw* 2020;20:e8.
28 Krishna S, Lowery FJ, Copeland AR, *et al*. Stem-like CD8 T cells mediate response of adoptive cell immunotherapy against human cancer. *Science* 2020;370:1328–34.
29 Jansen CS, Prokhnevska N, Master VA, *et al*. An intra-tumoral niche maintains and differentiates stem-like CD8 T cells. *Nature* 2019;576:465–70.
30 Miller BC, Sen DR, Al Abosy R, *et al*. Subsets of exhausted CD8$^+$ T cells differentially mediate tumor control and respond to checkpoint blockade. *Nat Immunol* 2019;20:326–36.
31 Siddiqui I, Schaeuble K, Chennupati V, *et al*. Intratumoral Tcf1$^+$PD-1$^+$CD8$^+$ T Cells with Stem-like Properties Promote Tumor Control in Response to Vaccination and Checkpoint Blockade Immunotherapy. *Immunity* 2019;50:195–211.
32 Tung C-W, Ziehm M, Kämper A, *et al*. POPISK: T-cell reactivity prediction using support vector machines and string kernels. *BMC Bioinformatics* 2011;12:446.
33 Montemurro A, Schuster V, Povlsen HR, *et al*. NetTCR-2.0 enables accurate prediction of TCR-peptide binding by using paired TCRα and β sequence data. *Commun Biol* 2021;4:1060.
34 Chronister WD, Crinklaw A, Mahajan S, *et al*. TCRMatch: predicting T-cell receptor specificity based on sequence similarity to previously characterized receptors. *Front Immunol* 2021;12:640725.